Journal of Marine Research, 55, 1–29, 1997

Journal of
MARINE RESEARCH

Volume 55, Number 1

Phytoplankton patches at fronts: A model of formation and response to wind events

by Peter J. S. Franks[1] and Leonard J. Walstad[2]

ABSTRACT

A subsurface patch of chlorophyll is a feature common to many fronts. The dynamics underlying the patch formation are not well understood; however, there appears to be a strong link between the biological and physical dynamics. Here we test the hypothesis that patch formation is a result of wind-forced motions of the front. Frontal responses to transient wind events include acceleration of the surface layers, changes in mixed-layer depth, and excitation of nonlinear oscillations at the front. Such dynamics can affect nutrient fluxes across the pycnocline and the coupling between trophic levels. To test this hypothesis, we developed a two-dimensional coupled mixed-layer/primitive-equation/ecosystem model, which we forced with transient wind events. We explored a range of initial conditions, including the cross-frontal nutrient gradient, the sinking of phytoplankton, the depth of the euphotic zone, and the depth of the front. The model showed the subsurface chlorophyll patch to be dependent on all these factors. The cross-frontal scale of the patch was found to be a historical artifact of past wind events, and so was not strongly related to the scale of the front (given by the Rossby radius of deformation). Winds aligned with the frontal jet weakened the cross-frontal density gradient, causing a flux of nutrients into the warmer waters of the front, and eroding the chlorophyll patch through deep vertical mixing. Winds aligned against the frontal jet enhanced the cross-frontal density gradient and isolated the subsurface patch from vertical mixing. The transient forcing of the fronts led to relatively high *f*-ratios in the subsurface patches; this enhanced biomass would be invisible to most satellite sensors.

1. Introduction

A biological feature associated with many fronts in the ocean is a subsurface patch of enhanced chlorophyll biomass on the stratified side of the front. Such features have been

1. Scripps Institution of Oceanography, University of California-San Diego, La Jolla, California, 92093-0218, U.S.A.

2. Horn Point Environmental Laboratory, Center for Environmental and Estuarine Studies, The University of Maryland System, P.O. Box 775, Cambridge, Maryland, 21613-0775, U.S.A.

seen at tidal fronts (e.g., Holligan, 1981; Pingree *et al.,* 1978), shelf-break fronts (e.g., Houghton and Marra, 1983), wind-driven upwelling fronts (e.g., Traganza *et al.,* 1987; Small and Menzies, 1981), eastern boundary currents (e.g., Hood *et al.,* 1991; Washburn *et al.,* 1991), western boundary currents (e.g., Lohrenz *et al.,* 1993; Hitchcock *et al.,* 1993) and the Almeria-Oran front of the Mediterranean (Claustre *et al.,* 1994a,b; Prieur and Sournia, 1994). The processes invoked to account for the formation and maintenance of such patches are diverse, and include: subduction of surface populations (Hood *et al.,* 1991; Claustre *et al.,* 1994a; Lohrenz *et al.,* 1993; Washburn *et al.,* 1991); physical accumulation (e.g., Boucher *et al.,* 1987; Franks, 1992b); enhanced growth in response to diapycnal or isopycnal nutrient fluxes (Yentsch, 1974; Hitchcock *et al.,* 1993; Holligan *et al.,* 1984; Traganza *et al.,* 1987); photoadaptation (Hood *et al.,* 1991; Claustre *et al.,* 1994b); and reduced grazing stress (e.g., Holligan *et al.,* 1984; Mitchell-Innes and Walker, 1991).

A finding common to all physical-biological studies of fronts is that phytoplankton production is strongly linked to physical forcing at time scales of weeks to months (e.g., Gulf Stream meanders, Hitchcock *et al.,* 1993; Lohrenz *et al.,* 1993; jets of the coastal transition zone, Washburn *et al.,* 1991; Hood *et al.,* 1991). However, the importance of transient events (days) to the phytoplankton dynamics at fronts is just beginning to be recognized (e.g., Claustre *et al.,* 1994b). Short time and space scale physical processes, for example wind events, can excite nonlinear phenomena which decouple biological trophic interactions. Such decouplings may lead to transient states in which the phytoplankton can show unusually high net production rates, leading to an amplification of phytoplankton patchiness at fronts.

Logistical limitations have allowed only limited sampling of the response of the phytoplankton community to episodic forcings such as wind events. Eppley and Renger (1988) happened to be sampling during a weak wind event, during which they measured a nanomolar increase in nitrate, followed by an increase in the rate of primary production. Klein and Coste (1984) modeled the response of the surface nutrient field to wind stress at the surface. They showed that the inertial oscillations of the surface waters led to pulses of nutrient input to the surface, as the water velocities were alternately opposed to and aligned with the wind stress. Eppley (1992) presented data showing a positive correlation of the f ratio (ratio of new/total production; Dugdale and Goering, 1967) with frequency of winds $\geq$10 knots in the Southern California Bight, suggesting a link between wind-driven nutrient transport and production. The spatial resolution of these observations, however, precluded analysis of the relationship of wind-forced production with submesoscale hydrographic features.

There have been several coordinated studies of the physics and biology of fronts. Most of those studies have been focused on coastal features such as tidal fronts or wind-driven upwelling. Only a few have examined oceanic fronts (e.g., Almofront-1, Prieur and Sournia, 1994; BIOSYNOP, Hitchcock *et al.,* 1993; CTZ, Brink and Cowles, 1991), and none has examined the role of transient wind events at fronts in mediating phytoplankton production in these physically dynamic regions. Logistical constraints and the difficulties in predicting and sampling during a wind event have left this problem largely unexplored.

As a first attempt at elucidating the processes coupling the physical dynamics and phytoplankton production at wind-perturbed fronts, we have developed a coupled primitive-equation/mixed-layer/ecosystem model. We apply this model to an idealized frontal region to explore the factors controlling the formation of subsurface patches at fronts, and the effects of transient wind events on these patches. We use this model in an heuristic sense: we seek to understand mechanisms of phytoplankton patch formation at idealized fronts under idealized forcing, rather than attempting to simulate a specific data set. The modeling results suggest that subsurface patches can form under appropriate conditions of frontal shape, euphotic depth, nutrient gradient, and grazing pressure. Wind events were found to alter the shape and relative production within the subsurface patches; the direction of the wind was important in determining the future patch characteristics. In general, subsurface patches of phytoplankton at fronts were a complicated function of historical properties and forcings.

2. Physical model

The physical model was based on that of Adamec *et al.* (1981), combining a primitive equation model with a bulk mixed-layer model (Garwood, 1977). Briefly, the governing equations for the two-dimensional flow were

$$\frac{\partial u}{\partial t} = -\frac{\partial (uu)}{\partial x} - \frac{\partial (uw)}{\partial z} + fv + A_m \frac{\partial^2 u}{\partial x^2} + K_m \frac{\partial^2 u}{\partial z^2} - \frac{\partial \overline{u'w'}}{\partial z} - \frac{1}{\rho_o}\frac{\partial p}{\partial x} \tag{1}$$

$$\frac{\partial v}{\partial t} = -\frac{\partial (vu)}{\partial x} - \frac{\partial (vw)}{\partial z} - fu + A_m \frac{\partial^2 v}{\partial x^2} + K_m \frac{\partial^2 v}{\partial z^2} - \frac{\partial \overline{v'w'}}{\partial z} \tag{2}$$

$$\frac{\partial \rho}{\partial t} = -\frac{\partial (\rho u)}{\partial x} - \frac{\partial (\rho w)}{\partial z} + A_h \frac{\partial^2 \rho}{\partial x^2} + K_h \frac{\partial^2 \rho}{\partial z^2} - \frac{\partial \overline{\rho'w'}}{\partial z} \tag{3}$$

$$\frac{\partial u}{\partial x} + \frac{\partial w}{\partial z} = 0 \tag{4}$$

$$\frac{\partial p}{\partial z} = -\rho g \tag{5}$$

$$\frac{\partial h}{\partial t} + \frac{\partial (hu)}{\partial x} = \frac{\partial h}{\partial t} + w_{-h} = w_e \tag{6}$$

where the variables are given in Table 1. The coordinate system was defined with x oriented across the front, y along the front, and z increasing upward. Gradients of properties along the front, $\partial()/\partial y$, were zero, implying no variation along the axis of the front. The rigid lid boundary condition was imposed at the surface ($w = 0$ at $z = 0$), requiring the divergence of the vertically averaged motion to be zero. In this model, the assumption was made that

Table 1. Parameters of the physical model.

Parameter	Definition
A_m	coefficient of horizontal eddy diffusion of momentum
A_h	coefficient of horizontal eddy diffusion of heat
h	mixing-layer depth
K_m	coefficient of vertical eddy diffusion of momentum
K_h	coefficient of vertical eddy diffusion of heat
f	Coriolis frequency
g	acceleration due to gravity
p	pressure
R	Rossby radius of deformation
T	temperature
u	horizontal velocity along x axis
v	horizontal velocity along y axis
w	vertical velocity along z axis
w_e	entrainment velocity at base of mixed layer
w_{-h}	vertical velocity just below base of mixed layer
x	cross-frontal horizontal coordinate
x_o	horizontal location of front at surface
y	along-frontal horizontal coordinate
z	vertical coordinate
z_o	depth of pycnocline away from front
z_p	thickness of pycnocline
τ_x	surface wind stress along x axis
τ_y	surface wind stress along y axis
ρ	density
ρ_o	reference density

the vertically averaged motion (the barotropic mode) itself was zero, implying that the vertical shear driven by the surface forcing was much greater than the dynamically induced barotropic motions.

The mixing layer depth, h, is a material surface with a specified cross-surface flux, the entrainment rate, w_e. The simplification shown in the prognostic equation for the mixing layer depth (6) is accomplished by requiring that the momentum, u, is independent of depth in the mixing layer, and by making use of the continuity equation (4) and the rigid lid boundary condition, $w = 0$ at $z = 0$. The entrainment velocity was parameterized according to the bulk second-order closure model of Garwood (1977, as described in Adamec *et al.*, 1981). If the turbulent kinetic energy flux was greater than the potential energy required for entrainment (given by the density gradient), the mixing layer would deepen. The values of the turbulent fluxes at the surface ($\overline{u'w'}$, $\overline{v'w'}$ at $z = 0$) were determined by the surface wind stress (τ_x, τ_y). No surface buoyancy flux ($\overline{\rho'w'}$) was used in this study.

The actively mixing layer was modeled as a slab, i.e. velocity, density and biological components were homogeneous throughout the mixing layer. A significant feature of the coupled primitive-equation/mixed-layer model was that the depth of the mixing layer did not have to correspond with any of the primitive-equation model's grid points—it was

continuously variable. The mechanism for this coupling is described in detail in Adamec *et al.* (1981).

Stable density and momentum profiles within and below the mixing layer were ensured by the use of a convective adjustment scheme based on the local gradient Richardson number. If the Richardson number fell below 0.25, then the buoyancy and momentum profiles were mixed until the Richardson number was slightly above 0.25. There was also a static stability criterion, which eliminated static instabilities by homogenizing adjacent grid points.

The model domain was 120 km wide by 500 m deep. The horizontal resolution of the model grid was 1 km, while the vertical resolution varied from 1 m in the top 50 m, to 100 m at the bottom (Fig. 1). The latitude was 30N (1 day inertial period), with no variation in f. This latitude was chosen more for numerical convenience than as a simulation of a specific location. The model results apply to most latitudes, with an appropriate scaling of the inertial period. The model was solved using centered space differencing on a staggered grid, with a time step of 300 s. No flux of mass or momentum was allowed through the bottom boundary, while open boundary conditions (Orlanski (1976) radiation condition, and $\partial(uu)/\partial x = \partial(vu)/\partial x = 0$) were specified at the lateral boundaries. The wind stress was specified at the surface, but no buoyancy forcing was used in this set of experiments. Lateral boundaries were far removed from the study area to ensure that there were no influences of the boundaries on the study area. The model structure and boundary conditions were tested by comparing the numerical result of a Rossby adjustment problem (e.g., Gill, 1982) to its analytical solution.

The initial density distribution was specified by analytical functions; the density was determined solely by the temperature with salinity constant everywhere. The horizontal dependence of the depth of an isopycnal followed a $(1 - e^{-(x - x_o)/R})$ distribution, where R was the Rossby radius of deformation and x_o the horizontal location of the front. The vertical distribution of isopycnals followed a $\tanh((z - z_o)/z_p)$ distribution, where z_o was the depth of the pycnocline, and z_p the scale for the pycnocline thickness (Fig. 2). A small linear increase of density with depth was also specified. Numerous experiments were conducted exploring the influence of these parameters on the model results, some of which will be described below.

The model was initialized with the specified density distribution assuming a geostrophic balance, giving a strong along-front jet and no initial cross-frontal circulation (Fig. 2). To eliminate initial transients, the model was allowed to evolve for five days before the application of the wind stress. Background values for eddy viscosities and diffusivities were specified for the regions below the mixing layer, and are given in Figure 1.

3. Biological model

The biological model was the simple nutrient-phytoplankton-zooplankton (*NPZ*) model of Franks *et al.* (1986) (Fig. 3). This model is often cited incorrectly as Wroblewski *et al.* (1988) (e.g., Fasham *et al.*, 1990; Steele and Henderson, 1992; Dippner, 1993; Ruan, 1993). The Franks *et al.* model uses nitrogen as a tracer for the state variables, assuming Michaelis-Menten kinetics govern the uptake of dissolved nutrients by phytoplankton, and

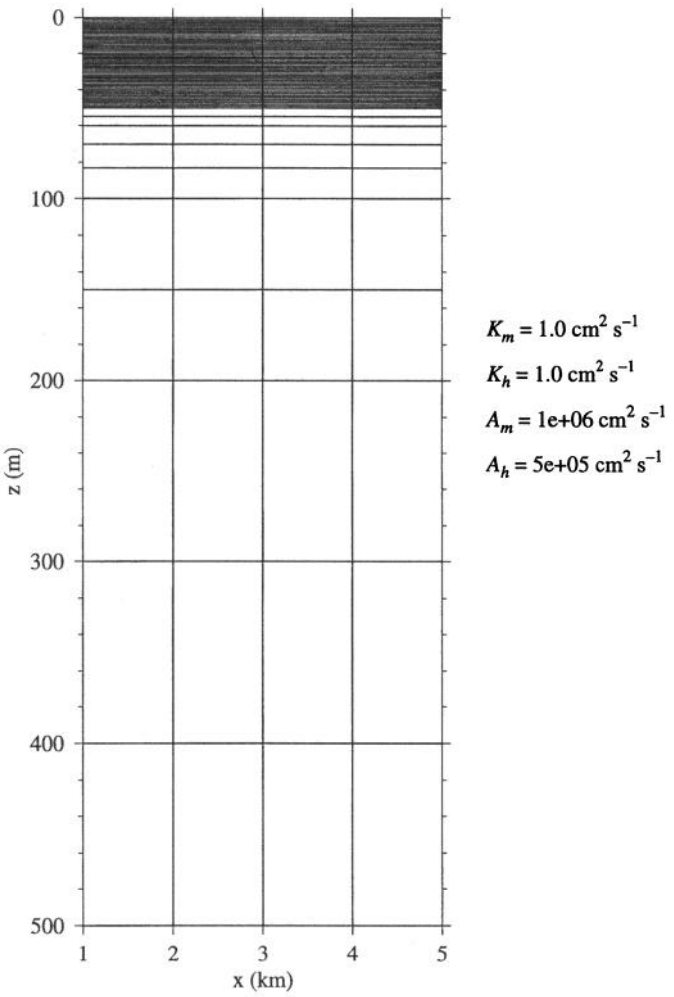

Figure 1. A portion of the model grid; each intersection represents a grid point. Horizontal resolution is 1 km. Vertical resolution varies from 1 m in the upper 50 m, to 100 m near the bottom. The domain is 120 km × 500 m, although only the upper 100 m are shown in the following figures. The background values for the eddy diffusivities of momentum and heat are also given.

an Ivlev grazing response of zooplankton to phytoplankton concentration:

$$\frac{dP}{dt} = \frac{V_m N}{k_s + N} f(I_o)P - ZR_m(1 - e^{-\lambda P}) - \epsilon P \tag{7}$$

$$\frac{dZ}{dt} = \gamma ZR_m(1 - e^{-\lambda P}) - gZ \tag{8}$$

$$\frac{dN}{dt} = -\frac{V_m N}{k_s + N} f(I_o)P + (1 - \gamma)ZR_m(1 - e^{-\lambda P}) + \epsilon P + gZ, \tag{9}$$

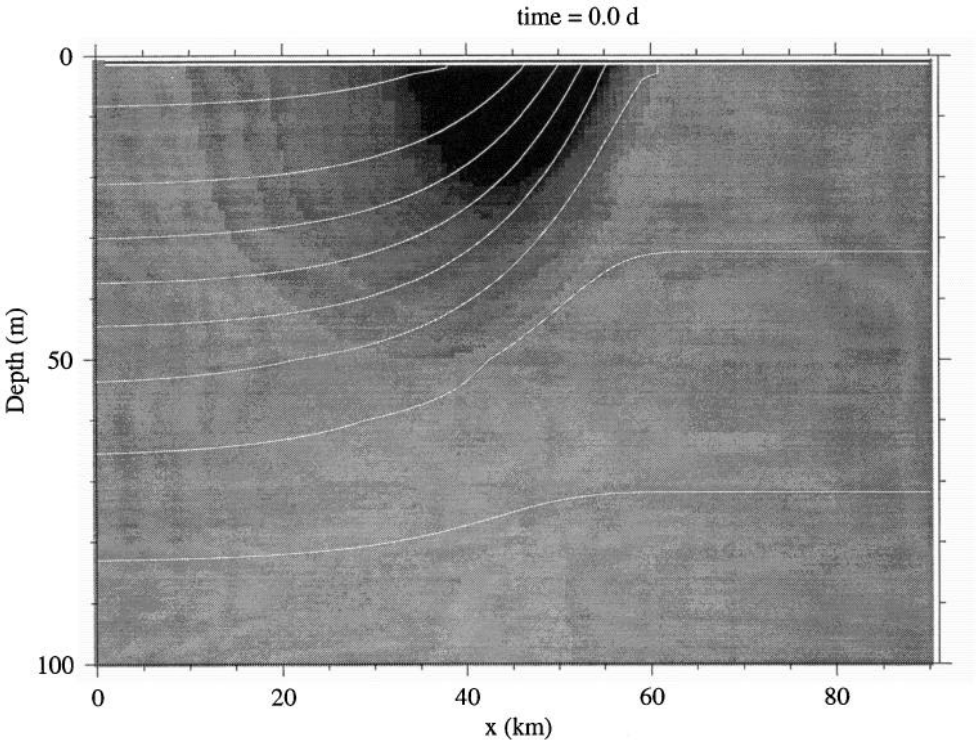

Figure 2. Physical initial condition. Thin white lines are isotherms, spaced every 1°C. Gray-scale shading is along-front velocity at geostrophic balance. Black indicates peak velocities of 70 cm s^{-1}, out of the page, induced by the geostrophic balance at the front.

where P is phytoplankton, Z zooplankton and N dissolved nutrient, all in μmole N l^{-1}. The total amount of nutrient, N_T, is conserved: $N + P + Z = N_T$. N_T is a property of the water mass when the model is initialized, thus gradients in N_T are advected and diffused like any passive tracer. If any state variable, such as phytoplankton, moves independently of the

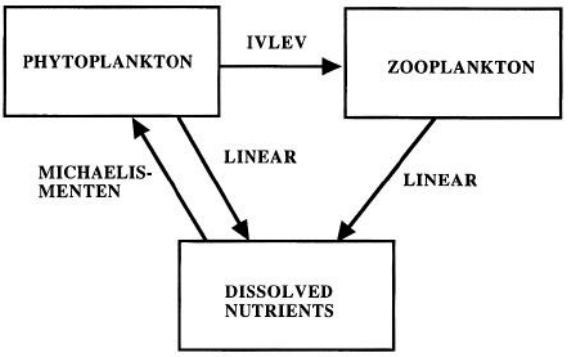

Figure 3. Biological model. Three compartments, phytoplankton (P), zooplankton (Z) and dissolved nutrients (N) are linked by the fluxes and types of kinetics indicated by the arrows.

Table 2. Parameters and their values used in the biological model.

Parameter	Definition	Value
V_m	maximum nutrient uptake rate	2.0 day^{-1}
k_s	half-saturation constant for nutrient uptake	0.1 μmole N l^{-1}
ϵ	death rate of phytoplankton	0.1 day^{-1}
R_m	maximum grazing rate	0.5 day^{-1}
λ	grazing efficiency	0.2 (μmole N l^{-1})$^{-1}$
γ	fraction of food assimilated	0.7
g	death rate of zooplankton	0.2 day^{-1}
k_{ext}	diffuse attenuation coefficient for irradiance	0.06–0.08 m^{-1}
N_T	total amount of nutrient ($P + Z + N$)	5–10 μmole N l^{-1}

water by sinking or swimming, then N_T will not be locally conserved, since a portion of N_T is moved separately from the remaining state variables.

There are seven parameters governing the Franks *et al.* model. The maximal phytoplankton nutrient uptake rate (and growth rate) is V_m, with a half-saturation constant k_s. The zooplankton have a maximal grazing rate R_m, with the grazing efficiency controlled by λ. Only a portion, γ, of the ingested phytoplankton is assimilated by the zooplankton, the remainder being recycled into dissolved nutrients. Both phytoplankton and zooplankton die at rates ϵ and g respectively. These dead fractions are immediately recycled into dissolved nutrients. The phytoplankton depend on incident irradiance I_o through the function $f(I_o)$ which we have taken to be linear in the irradiance:

$$f(I_o) = I_o e^{-k_{ext}z} \tag{10}$$

where k_{ext} is the diffuse attenuation coefficient for irradiance and z is depth below the surface. No dependence of k_{ext} on the local particle (phytoplankton) concentration was included. The parameter values were chosen for an arbitrary oceanic ecosystem, based on the range of values suggested by Franks *et al.* (1986) (Table 2). A range of k_{ext} values was explored in the model.

The *NPZ* model of Franks *et al.* (1986) has an analytical steady-state solution which was used to initialize the coupled physical-biological model (Fig. 4). Thus during the model runs, any changes in the biological state variables must have been caused by physical forcings, allowing a clear separation of physical and biological dynamics in the formation of biological features. Since there is no dependence of any state variable on temperature, and no variation in k_{ext} across the front, there is no horizontal dependence of the initial condition for the biological state variables. To explore the effects of a cross-frontal nutrient gradient, numerous model runs were performed in which the total amount of nutrient, N_T, was varied across the front. This was accomplished by increasing N_T for temperatures $<12°C$ by some fraction between 1 and 2, creating a gradient in biological properties across the 12°C isotherm. Because the phytoplankton concentration at steady state is controlled by the zooplankton grazing (Franks *et al.*, 1986), the change in N_T across the front did not lead to significant changes in phytoplankton concentration across the front.

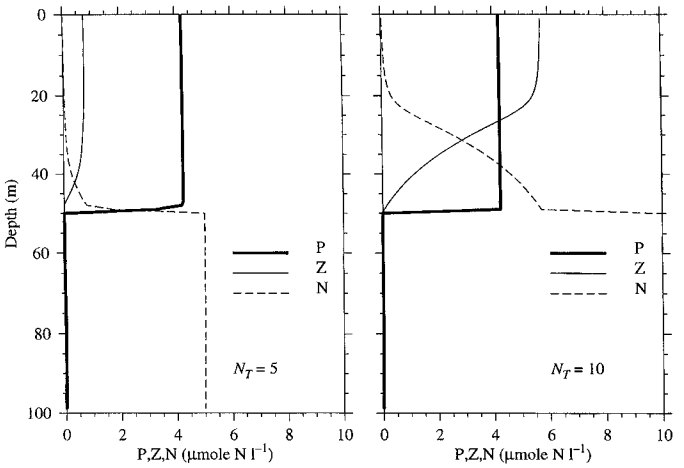

Figure 4. Biological initial conditions. Left panel: vertical profiles of P, Z and N at $t = 0$ for N_T = 5 μmole N l^{-1}. Right panel: vertical profiles for N_T = 10 μmole N l^{-1}. The right panel shows the vertical distribution of biological properties for the cases in which N_T was doubled in waters <12°C (see text). The phytoplankton growth rate decreases exponentially with irradiance, leading to a decreasing zooplankton biomass with depth. The decrease in zooplankton biomass is balanced by an increase in dissolved nutrients, while the phytoplankton biomass is constant throughout the euphotic zone.

The strongest cross-frontal gradients were those of the dissolved nutrient pool, which showed higher values on the cold side of the front at a given depth. Such gradients are commonly seen across fronts in temperate waters (e.g., Coastal Transition Zone, Chavez *et al.*, 1991; Almeria-Oran Front, Bianchi *et al.*, 1994; shelf-slope fronts, Marra *et al.*, 1990; Skagerrak/Kattegat fronts, Heilmann *et al.*, 1994), but are less pronounced at more tropical fronts (e.g., Azores Front, Fasham *et al.*, 1985).

4. No wind forcing

Physical. In the five days before wind forcing was applied, the model front relaxed due to the background diffusion. This relaxation created a weak double-celled cross-frontal circulation (Fig. 5). In the front, upwelled water was moved to the warm side of the front. Weak downwelling on the cold side of the front created a horizontal shear in the vertical velocity at the front. The maximal upwelling velocities were about 2 m day^{-1}. Since there was no wind stress or surface buoyancy flux, the mixed-layer model did not contribute to the dynamics at this stage of the model run.

Biological. The adjustment of the physical fields before the onset of the wind had the potential of influencing the biological dynamics through nutrient transport and the interaction of sinking organisms with the cross-frontal flows. To explore the range of possible dynamics, numerous cases were run using different pycnocline depths z_o, different

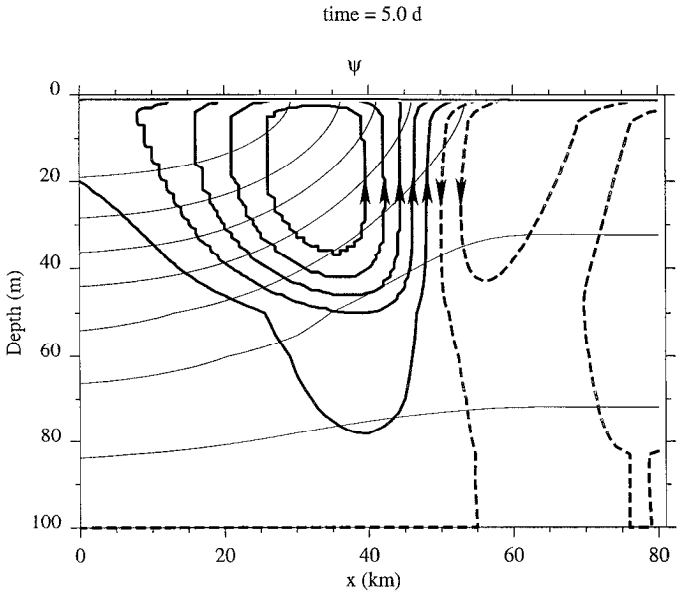

Figure 5. Cross-frontal stream function at day 5 generated by the relaxation of the initial temperature distribution. Maximum vertical velocities at the front were about 2 m day^{-1}. Water flowed along streamlines in the direction indicated.

extinction coefficients k_{ext}, different cross-frontal nutrient gradients of N_T (Fig. 6), and sinking *versus* nonsinking phytoplankton.

The formation of a subsurface phytoplankton patch at the front was strongly dependent on the interplay between the depth and strength of the nutrient gradient *versus* the magnitude of the diffuse attenuation coefficient for irradiance. Subsurface patches formed on the stratified side of the front centered at depths of about $1.5/k_{ext}$ if the nutrient gradient was sufficiently strong. The vertical extent (thickness) of the patch was greater for stronger cross-frontal nutrient gradients: about $0.5/k_{ext}$ for a 1.5 increase in N_T, and $1.3/k_{ext}$ for a 2-fold increase in N_T.

The formation of the subsurface patch depended on the physical transport of nutrients from below into the lower portion of the euphotic zone through diapycnal diffusion and advection. These nutrients were taken up by the phytoplankton, which were growing at a very slow rate (~0.15 day^{-1}) due to light limitation. The slow growth of the phytoplankton and the long response time and low local biomass of the zooplankton led to an uncoupling of the phytoplankton growth and the zooplankton grazing, allowing the local phytoplankton biomass to increase (e.g., Fig. 7). Stronger gradients in N_T led to increased cross-pycnocline transport into the euphotic zone combined with a decrease in nutrient stress, and correspondingly increased phytoplanktonic growth rates. Similar nutrient transport nearer the surface did not lead to an increase in phytoplankton biomass, rather, the increased phytoplanktonic growth rate led to increases in the zooplanktonic grazing and

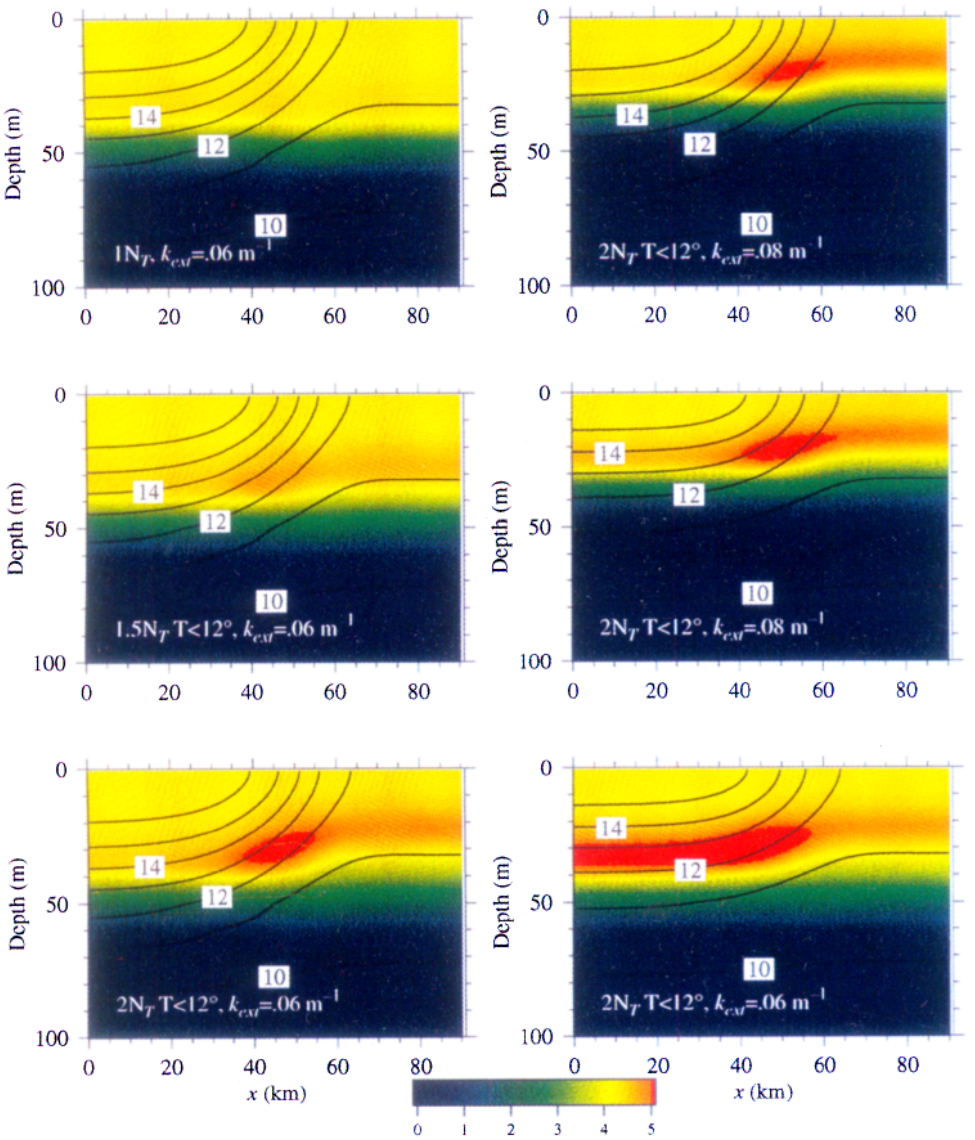

Figure 6. Phytoplankton fields at day 5 for six different initial conditions, as indicated on the panels. Temperature (°C) is indicated by solid black contours. Note that the pycnocline is shallower for the two lower right-hand panels. Phytoplankton concentration is given by the color bar at the bottom in units of μmole N l^{-1}; red values are >5. "$2N_T\,T < 12$°C" indicates that the total nutrient N_T was doubled for temperatures <12°C. The vertical diffuse attenuation coefficient for irradiance, k_{ext}, is indicated in each panel.

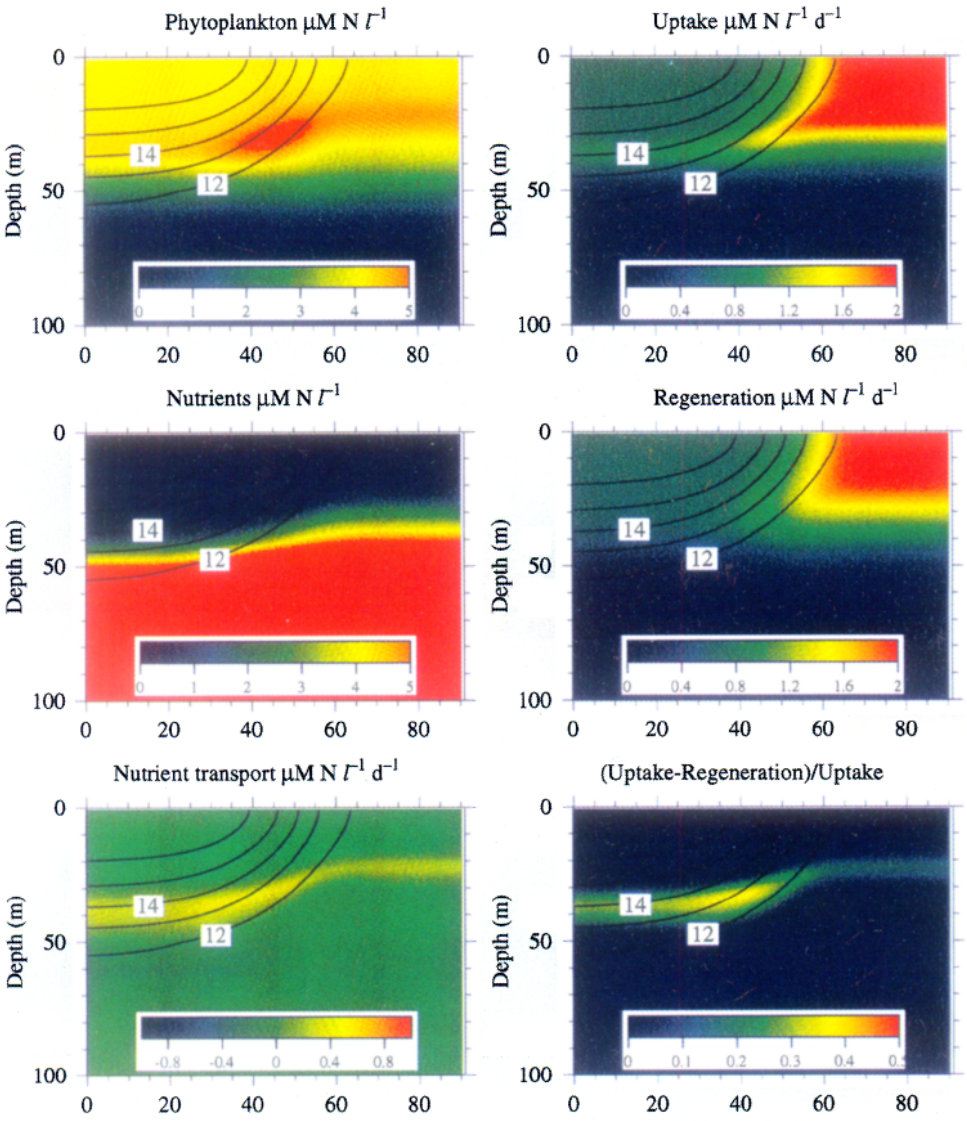

Figure 7. Term balances at day 5 for the case with $2N_T$ cross-frontal nutrient gradient and k_{ext} = 0.06 m^{-1}. In the lower left panel, positive values of nutrient transport are to the right or upward, while negative values are to the left or downward. Right panels refer to dissolved nutrient fluxes. The lower panel gives the fraction of total nutrient uptake *not* accounted for by regeneration and is similar to an *f* ratio. Color scales are indicated in each panel.

recycling rates. In this upper region of the euphotic zone the phytoplankton and zooplankton are more tightly coupled due to their high growth rates, responding quickly to any perturbations in the biological rates. The subsurface patch was delimited horizontally due to the upward curvature of the front: in the stratified waters the nutrients diffusing vertically through the pycnocline did not reach the euphotic zone, so phytoplankton showed no uncoupled growth. On the cold side of the front, the cross-frontal nutrient flux occurred mainly at the top of the euphotic zone, where grazing limited phytoplankton biomass. The nutrient flux across the curved portion of the pycnocline, however, was sufficiently shallow to stimulate phytoplankton growth in the euphotic zone, but sufficiently deep to allow phytoplankton growth to be uncoupled from grazing. Thus, in the unforced case, the horizontal extent of the subsurface phytoplankton patch was controlled by the interaction of the light attenuation, cross-frontal nutrient gradient, depth of pycnocline, curvature of the pycnocline and grazing pressure.

The balance of terms shown in Figure 7 indicates that the nutrient uptake rate of the phytoplankton exceeds the regeneration rate by zooplankton in the subsurface patch. The ratio of (uptake-regeneration)/uptake gives the proportion of total uptake *not* accounted for by regenerated nutrients: a value comparable to an *f* ratio (Dugdale and Goering, 1967). There is an exact correspondence of high ($\sim$0.4) values of this ratio with the region of enhanced vertical nutrient transport at the front, indicating that the excess nutrients are being supplied to the subsurface patch physically rather than biologically.

The spatial variation in vertical velocities at the front gives the potential for accumulation of sinking or swimming biomass at the front (e.g., Franks, 1992b). To investigate this possibility, we allowed sinking of the phytoplankton, with a constant speed w_s. The use of constant sinking speed will not allow accumulation, i.e. the Lagrangian concentration of phytoplankton (following a phytoplankton cell) will not change due to physical effects (as discussed in Franks, 1992b). However, the residence time in the euphotic zone may change, due to sinking cells slowing in the upwelling regions. This increased residence time may lead to biological dynamics contributing to the formation of subsurface patchiness of phytoplankton. At a sinking speed of 1 m day^{-1}, however, no significant horizontal patchiness was created (Fig. 8). Any upwelling-forced slowing of the sinking speed was compensated by an increase in the physically forced horizontal velocities, moving cells away from the front. Thus only slight horizontal gradients were created where cells were downwelled on the cold side of the front, and upwelled within the front. The interaction of constant sinking with the weak cross-frontal circulation, then, would not allow the formation of a subsurface phytoplankton patch at this front.

5. Wind forcing

Physical. After five days of relaxation, a wind stress was applied to the front. This wind stress was of 0.5 day duration, with a Gaussian ramp and decay of standard deviation 0.2 day (Fig. 9). The windstress was spatially uniform over the water's surface. Many different wind stresses were tested, varying the duration, magnitude and direction of the stress. As a

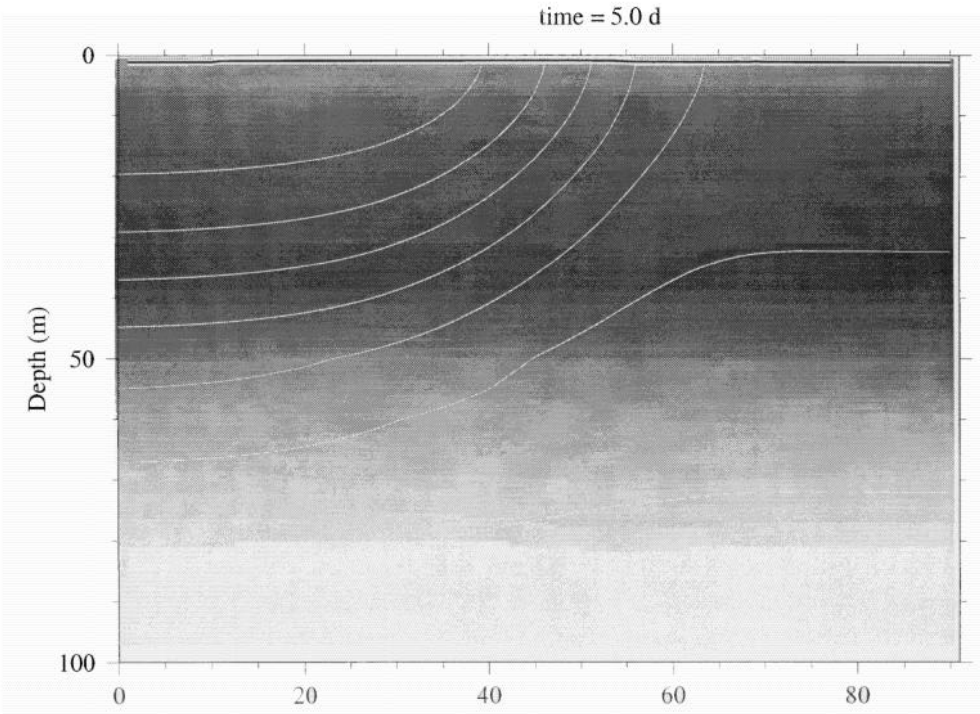

Figure 8. Phytoplankton field at day 5. Phytoplankton were sinking at 1 m day $^{-1}$, and there was no cross-frontal nutrient gradient. There is only a weak signal of the interaction between the sinking phytoplankton and cross-frontal flows.

standard case, the maximal magnitude was set to 0.2 Pa (=N m^{-2}). Two representative wind directions will be explored in detail below: both are along the front (y axis), but in opposite directions. When the stress is positive ($\tau_y > 0$) the surface Ekman flux is toward the cold side of the front, and the wind stress opposes the direction of the geostrophic jet. When $\tau_y < 0$, the Ekman flux is toward the warm side of the front, and the wind stress is aligned with the frontal jet. For all the wind-forced cases discussed below, the pycnocline was centered at 40 m on the stratified side of the front.

During the wind event, the mixed layer deepens as a function of the magnitude and duration of the wind stress and the local vertical gradient of density (Fig. 10). The detailed time series of Figure 10 shows deeper mixed-layer depths on the cold side of the front where the stratification is weaker. The initial rate of deepening is quite fast, but slows due to the increased vertical distance over which mixing must be accomplished, and to the increased density gradient at the base of the mixed layer as the mixed layer thickens.

The surface waters are gradually accelerated to the right of the wind, with higher velocities in the thinner warm water layer. The cross-frontal divergences and convergences created by the horizontal velocity ($\partial u/\partial x$) across the front oscillate at the Coriolis frequency, f. These horizontal divergences and convergences create upwelling and down-

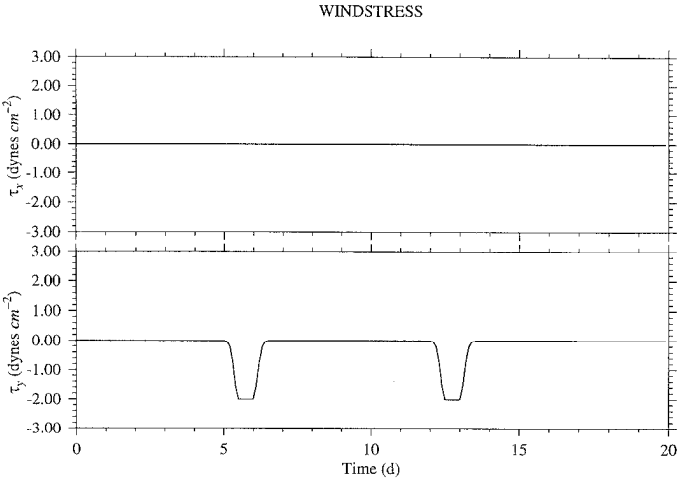

Figure 9. Magnitude and timing of surface wind stress. No wind stress was applied in the x-direction (across-front; top panel). Two wind events were applied in the along-front direction (bottom panel), with a maximum stress of 0.2 Pa (2 dynes cm^{-2}). The along-front wind stress was applied in both the positive y (into the page) and negative y (out of page) directions.

welling at the front which also oscillate at the inertial frequency—inertial pumping (Price, 1983). Maximum upwelling velocities are about 45 m day^{-1}, but that rate is sustained for only a short time during the inertial oscillations. This inertial pumping gradually decays after the wind event, but is still evident after 15 days. The inertial oscillations are 180° out of phase when the wind stress is applied in the opposite direction.

Wind forcing accelerates the mixed layer in the direction of the wind, and this flow is then turned to its right by the Coriolis force, fu^w, where u^w is the directly wind-driven component of the flow. As the flow is turned to its right, it begins to transport the vorticity of the front. Because the vorticity of the front is comparable to f, this term enters significantly into the vorticity balance. As a result, the magnitude and oscillation period of the wind-driven flow depend upon the local vorticity. The wind-driven flow will be divergent despite the absence of curl in the wind stress, and this divergence will depend upon the direction of the wind stress (Niiler, 1969). This behavior is not specific to two-dimensional fronts, but is a general feature of ocean flows (Walstad and Robinson, 1993).

Because both the period and amplitude of the response are dependent upon the local vorticity, there are two components of the vertical velocity. Horizontal gradients in the period of the response generate oscillating vertical velocities, while the horizontal gradient in the amplitude of the response generates a mean vertical velocity. Though the precise vertical velocities depend on the gradient of the relative vorticity, we can identify these velocities for a front which has a horizontal peak of vorticity located near the front, and decreases monotonically away from the front. With the wind blowing in the direction of the

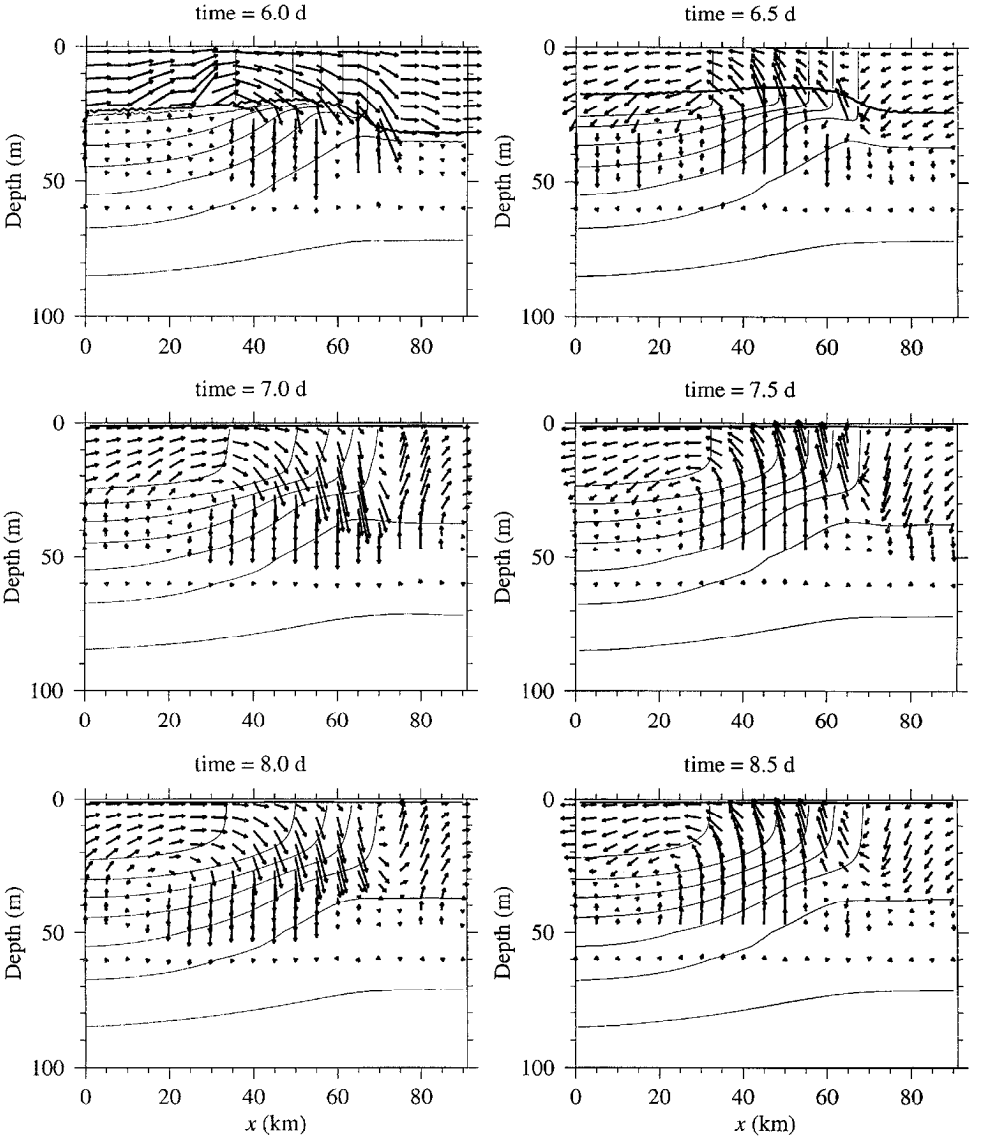

Figure 10. Time series of cross-frontal velocities (arrows) and temperature (thin lines) during and after a wind event in which $\tau_y > 0$ (into page). The mixing-layer depth is indicated by the heavy solid line. Times are indicated at the top of each panel; the time interval is half an inertial period. Arrows are drawn at every fifth grid point vertically and horizontally. Time series of wind stress is given in Figure 9. Note the alternation of upwelling and downwelling at the front at the inertial time scale.

flow, the vertical velocity at the base of the mixed layer will be downward on the edges of the jet, and upward in the middle of the jet. With the wind blowing in the opposite direction, the vertical velocities are reversed. The amplitude of the cyclic pumping is independent of wind direction. Both components are important to the biology, as they move water into and out of the euphotic zone. Nonlinear processes in the physical environment make both components important to the frontal mixed-layer dynamics as well.

There are subtle but important differences in the physical dynamics forced by $\tau_y > 0$ and $\tau_y < 0$ (Fig. 11). When the Ekman flux is from the cold side to the warm side of the front ($\tau_y < 0$), the depth of the mixed layer increases monotonically from the warm side to the cold side. Cross-frontal mixing is enhanced at the front as cold (dense) water is forced over warmer water. The static instabilities created then generate vertical mixing and a substantial diapycnal flux across the front within the mixed layer. The vertical density gradient is generally decreased by this mixing, leading to weaker stratification at the front.

In contrast, when the Ekman flux is from the warm side to the cold side of the front ($\tau_y > 0$), the stratification at the front is increased. This enhanced vertical density gradient suppresses the vertical mixing, creating a shallow mixed layer at the front, with deeper mixing on either side. There is little cross-frontal mixing, since the wind tends to enhance the density gradients.

These results could not have been obtained with a one-dimensional model, or with a two-dimensional primitive-equation model without the mixed-layer model. These cross-frontal asymmetries are inherently two and three-dimensional processes, coupling the horizontal advection of density gradients with the vertical mixing due to a surface wind stress. The importance of these dynamics to the biological processes will be described below.

Biological. For each of the two wind directions described above, four biological cases will be discussed below: (1) no sinking, no nutrient gradient; (2) no sinking, $2N_T$ nutrient gradient (Fig. 12); (3) sinking, no nutrient gradient (Fig. 13); (4) sinking, $2N_T$ nutrient gradient (Fig. 14). The nutrient gradient was created in the same manner as described above for the unforced case (N_T was increased by $2\times$ for temperatures $<12°C$). In the cases with sinking, only phytoplankton were allowed to sink, at a constant velocity of 1 m day^{-1}. For all the biological cases discussed below, the light extinction coefficient, k_{ext}, was set at 0.06 m^{-1} (see Fig. 6).

a. Case 1: no sinking, no nutrient gradient

In case 1 with no sinking and no nutrient gradient across the pycnocline, there was very little response of the phytoplankton to the wind event, and no obvious difference between the runs with wind forcing from opposite directions. A slight increase in phytoplankton biomass occurred at the base of the euphotic zone as nutrients diffused upward before the wind event. During the wind event, this local increase was homogenized throughout the mixed layer, leaving a horizontally uniform phytoplankton field. The inertial oscillations at the front after the wind event led to a slight increase (~0.1 μmole N l^{-1}) in phytoplankton

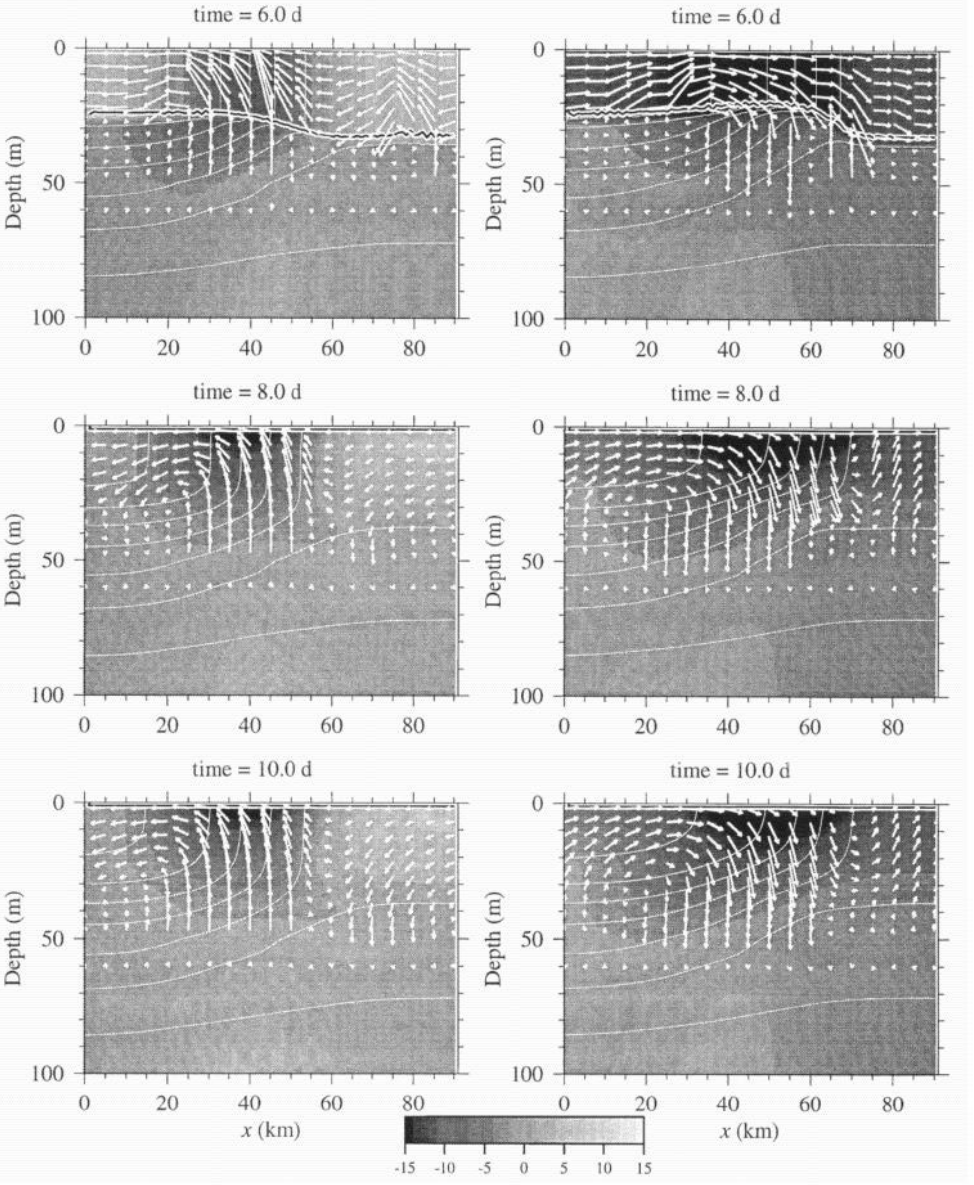

Figure 11. Time series of cross-frontal velocities (arrows), temperature (thin white lines), mixing-layer depth (solid black and white line), and along-front velocities (gray scale) for wind events with $\tau_y < 0$ (out of page; left panels) and $\tau_y > 0$ (into page; right panels). Times are indicated at the top of each panel. Gray-scale bar at bottom is in cm s^{-1}; negative values are out of the page. These are instantaneous snapshots of an oscillating field. Thus, the cross-front and along-front velocities are not in a steady-state balance and should not be interpreted as time-averaged fields. The inertial oscillations of the surface layer lead to the frontal jet alternately aligned with (left panels) and opposed to (right panels) the wind stress.

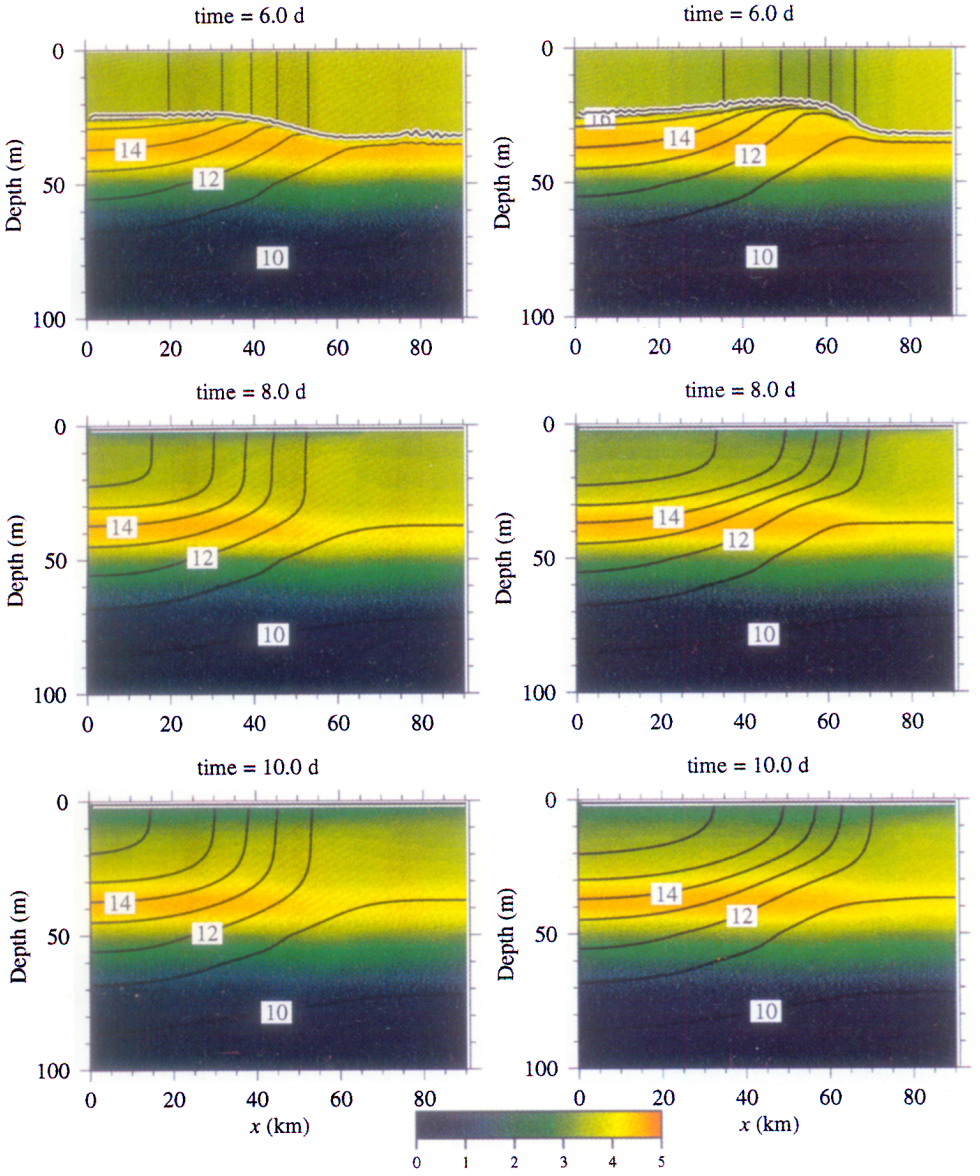

Figure 12. Time series of phytoplankton concentration (color scale, μmole N l^{-1}), temperature (black lines) and mixing-layer depth (solid black and white line) for wind events with $\tau_y < 0$ (out of page; left panels) and $\tau_y > 0$ (into page; right panels). Case 2: no cross-frontal nutrient gradient, phytoplankton sink at 1 m day^{-1}. Times are indicated at the top of each panel. Physical fields are given in Figure 11.

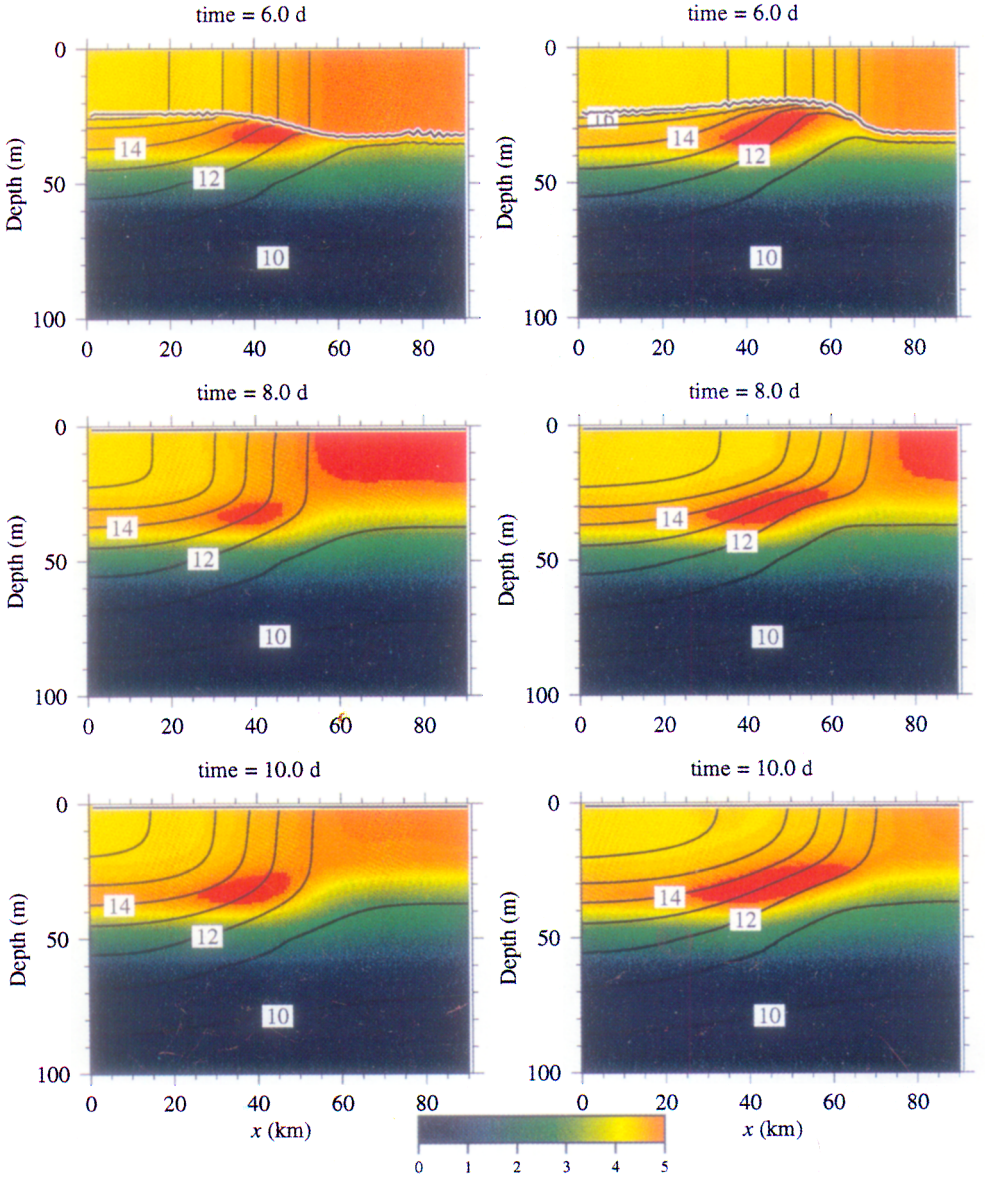

Figure 13. Legend same as Figure 12, but Case 3: $2N_T$ for $T < 12$°C cross-frontal nutrient gradient, no phytoplankton sinking.

biomass at the front at the base of the euphotic zone four days after the wind event. This weak patch of phytoplankton was created by the uplifting of nutrient-rich, phytoplankton-poor water into the euphotic zone by the inertial pumping, rather than a diapycnal flux of nutrients into the euphotic zone. The inertial pumping thus effectively increased the euphotic depth at the front (e.g., Holloway and Denman, 1989).

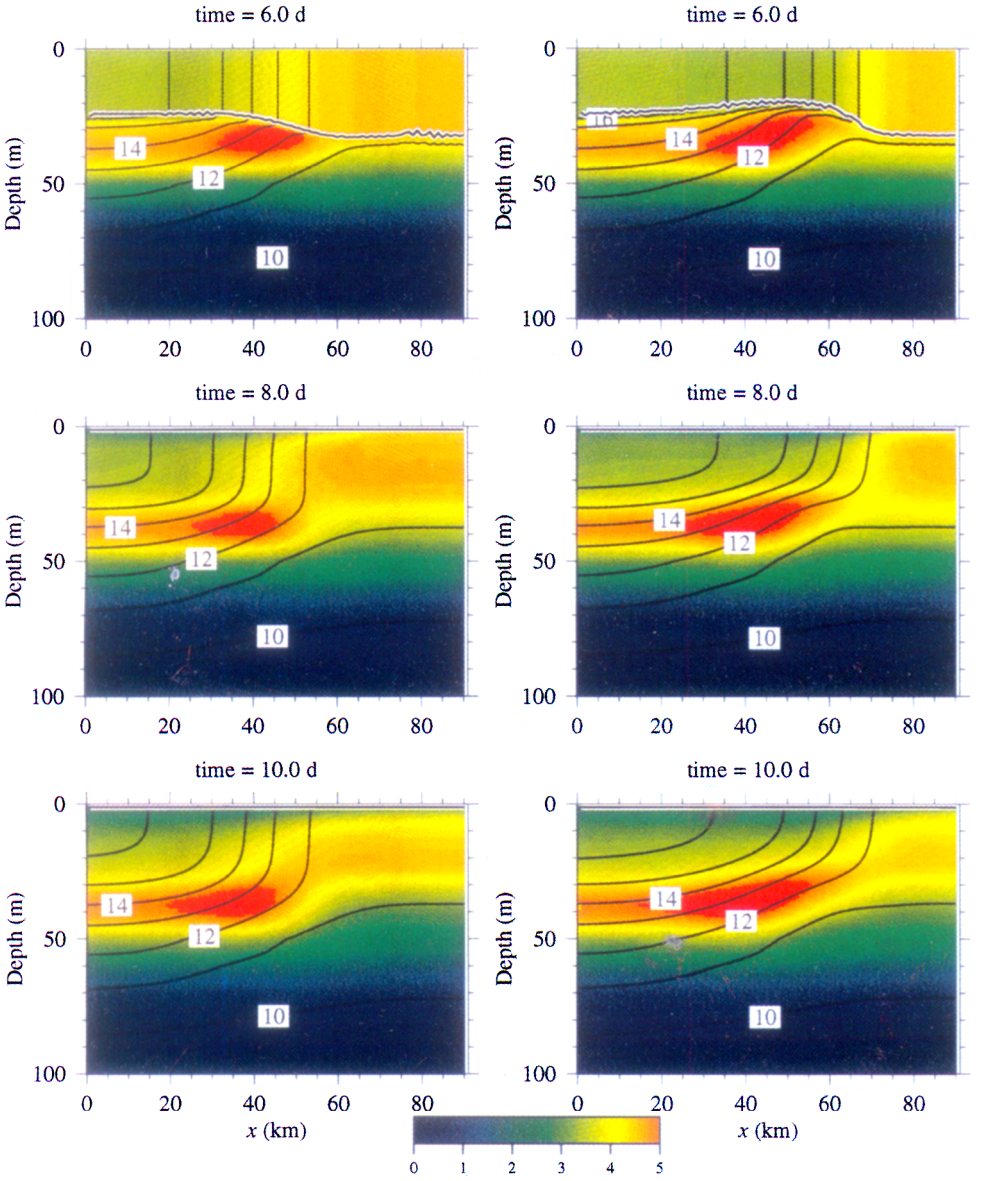

Figure 14. Legend same as Figure 12, but Case 4: $2N_T$ for $T < 12$°C cross-frontal nutrient gradient, phytoplankton sink at 1 m day^{-1}.

b. Case 2: sinking, no nutrient gradient

With sinking of phytoplankton added to case 1, a strong subsurface phytoplankton biomass maximum developed at about 35 m depth ($2.1/k_{ext}$) (Fig. 12). During the wind event, this subsurface maximum was eroded on the cold side of the front, and homogenized into the mixed layer. Because of the weakened stratification during the $\tau_y < 0$ case (Ekman

flux from cold to warm side of the front), the subsurface phytoplankton maximum was more thoroughly eroded at the front than in the $\tau_y > 0$ case. In both cases, the wind event left behind a subsurface phytoplankton maximum layer on the stratified side of the front which was strongly delimited horizontally by the front itself. The biomass within the subsurface maximum at the front was not significantly affected by the physical processes occurring at the front. The inertial pumping had the same weak effect on the biomass described above for the nonsinking case.

c. Case 3: no sinking, nutrient gradient

The strong nutrient gradient ($2N_T$ for $T < 12°C$) in this case led to a subsurface patch of phytoplankton biomass prior to the wind event (Fig. 6). During the wind event, the mixed layer eroded the shoalest portion of this patch, more strongly when $\tau_y < 0$ than $\tau_y > 0$ (Fig. 13). When the Ekman flux forced warm water over cold ($\tau_y > 0$), the consequent increase in vertical stratification protected the subsurface phytoplankton maximum from being mixed into the surface layer. Thus after the wind event an isolated subsurface patch of phytoplankton remained at the front, with a larger horizontal dimension in the $\tau_y > 0$ case.

Vertical mixing on the cold side of the front brought nutrients up into the euphotic zone, creating a strong phytoplankton bloom at the surface in the colder waters. This vertical transport continued after the wind event due to mixing allowed by low Richardson numbers on the cold side of the front. The very weak vertical stratification there was easily mixed by the vertical shear created by the inertial oscillations near the front. The horizontal cross-frontal mixing in the $\tau_y < 0$ case, forced by density instabilities as cold water was driven over warm, led to a nutrient flux from the cold to the warm side of the front. The consequent surface phytoplankton bloom was thus more pronounced in and near the front in this case than in the $\tau_y > 0$ case. Within four days after the wind event, grazing had reduced the phytoplankton biomass in the surface colder waters to near their original values, leaving only the isolated subsurface phytoplankton patch within the front as an obvious biomass maximum. This patch continued to grow in spatial extent as nutrients diffused across the pycnocline into the deep portion of the euphotic zone.

d. Case 4: sinking, nutrient gradient

The dynamics of this case were very similar to those of case 3, although the sinking of the phytoplankton led to a much more pronounced subsurface phytoplankton biomass maximum (Fig. 14). Once again, the wind events mixed nutrients up from below the euphotic zone on the cold side of the front, leading to a phytoplankton bloom in those waters after the wind event. This bloom was quickly grazed down by the zooplankton, leaving the subsurface patch of phytoplankton at the front as the most obvious biological feature. This patch was larger and more pronounced in the $\tau_y > 0$ case, as the increased stratification prevented erosion of the patch during mixed-layer deepening. The strong

horizontal gradients of phytoplankton at the surface after the wind event were in exactly the opposite sense of the subsurface horizontal gradients.

6. Discussion

Using a coupled primitive-equation/mixed-layer/ecosystem model we have shown that the formation and maintenance of subsurface patches of phytoplankton at fronts is strongly dependent on water-column properties (frontal characteristics, nutrient gradient, euphotic depth) and historical wind stress. The phytoplankton responded to cross-frontal nutrient fluxes and wind-driven vertical mixing and advection over relatively short time spans (~5 days). To first order, the phytoplankton dynamics at the wind-perturbed front were controlled by vertical fluxes of nutrients; however, details of the shape and biomass of the subsurface patch, and the cross-frontal fluxes of nutrients were strongly influenced by the wind direction. Winds with Ekman fluxes from the cold to the warm side of the front tended to erode the subsurface patch, and cause enhanced cross-frontal mixing leading to phytoplankton growth in the surface waters of the front. Winds causing Ekman fluxes from the warm to the cold side of the front created enhanced vertical stratification, leading to isolation of the subsurface patch, and little cross-frontal transport.

The phytoplankton growth under wind forcing was very patchy in time and space. The surface phytoplankton biomass was strongly controlled by the vertical transport of nutrients during wind events. This led to pronounced, transient blooms of phytoplankton in the colder water mass. The warm boundary of this bloom depended on the wind direction through its control on the cross-frontal nutrient flux. Much of the phytoplankton response, however, occurred at several optical depths below the surface (1 optical depth = $1/k_{ext}$), within the front. This production was horizontally limited by the curvature of the front, which controlled the relation of the nutrient gradient to the euphotic depth. The scale of the subsurface patches was not obviously related to the scale of the front after wind forcing (cf. Franks, 1992a). Winds driving cold water over warm water ($\tau_y < 0$) tended to reduce the scale of the patches by mixing the phytoplankton into the surface waters of the front. When $\tau_y > 0$, the patches became elongate as the front was driven over them. These scale changes were quite abrupt in time (~2 days), suggesting that wind forcing can be an important determinant of the scales of phytoplankton patchiness at fronts.

Production in the subsurface patches was driven by diapycnal advection and diffusion of nutrients, and by vertical oscillations at the front after the wind event which brought nutrient-rich waters into the euphotic zone. The f ratios of the patches (~0.4) were enhanced over the background values ($f < 0.1$), indicating that the patches were sites of new production (Dugdale and Goering, 1967; Eppley and Peterson, 1979). This is consistent with hypotheses of patch formation due to diapycnal nutrient fluxes (Yentsch, 1974; Hitchcock *et al.,* 1993; Holligan *et al.,* 1984; Traganza *et al.,* 1987; Claustre *et al.,* 1994b; Videau *et al.,* 1994). Waldron and Probyn (1991) found f ratios of 0.29–0.35 in the Benguela upwelling, which were low compared to values found by Kokkinakis and Wheeler (1987) off Oregon, or Eppley *et al.* (1979) off southern California ($f > 0.75$).

These latter values were measured in areas associated with strong wind-driven upwelling and high ambient nitrate concentrations. The present model does not describe a wind-driven upwelling system, but an existing frontal system under the influence of wind. Thus elevated *f* ratios at the model front are not necessarily expected *a priori;* they arise through the influence of wind-forced frontal dynamics on existing nutrient gradients.

The strongest test of this model would be a careful comparison to appropriate data collected across a front during and after a wind event. A thorough search of the literature did not reveal any such data sets. Cross-frontal transects with biological data almost always lacked wind information, and data sets with detailed physical information generally lacked biological fields (e.g., FASINEX, Weller, 1991; and particularly the wonderful physical data set of Eriksen *et al.,* 1991). Still, the patterns generated by the model can be interpreted in light of patterns at oceanic fronts, even in the absence of full physical and biological data sets. The weak response of the modeled phytoplankton to wind events when there was a small cross-frontal nutrient gradient (cases 1 and 2) suggests that similarly weak patch structures and cross-frontal gradients would be found at such fronts in the ocean. In studies of the Azores front, Fasham *et al.* (1985) and Karhu *et al.* (1991) did not find consistent enhancement of chlorophyll at the front. Cross-frontal nitrate gradients were small (<1 μM at 50 m), and cross-frontal differences in the depth of the deep chlorophyll maximum could be explained by differences in the *in situ* irradiance field. The larger diffuse attenuation coefficient in the east Atlantic water was presumed due to higher levels of integrated chlorophyll, fueled by wintertime mixing into a shallower nutricline than in the west Atlantic waters. Wind stresses acting on such a front would not be expected to promote subsurface patchiness of chlorophyll at the front, based on the present model.

Probably the best cross-frontal transects to compare to the model cases 3 and 4 (cross-frontal nutrient gradient and sinking) are station lines A and C of Hood *et al.* (1991), and repeated transects of line D of Chavez *et al.* (1991). These transects crossed a frontal jet off northern California during and after periods of sustained winds >10 m s^{-1} (Kosro *et al.,* 1991; Huyer *et al.,* 1991). The front forming the jet was created during wind-driven coastal upwelling, however the front was perpendicular to the coast, and far enough offshore (60–100 km) and removed from the upwelling region that local wind effects may have acted on the front as in the present model. The cross-frontal nitrate gradients were similar to those used in the $2N_T$ cases, being >4 μM on the cold side of the front and <0.5 μM on the warm side at 50 m depth. The winds were generally cross-frontal, with the Ekman flux directed along the jet axis (Huyer *et al.,* 1991; Kosro *et al.,* 1991). Dewey and Moum (1990) and Dewey *et al.* (1991) found that wind-driven vertical mixing in this frontal region led to greater penetration through the pycnocline in the colder waters of the front due to their proximity to the surface. This would promote the vertical mixing of nitrate, as in the present model, leading to phytoplankton blooms on the cold side of the front as in Figures 13 and 14 (upper and middle panels). Such a distribution of phytoplankton was observed on all such transects (Chavez *et al.,* 1991; Hood *et al.,* 1991). However, the coastal upwelling origin of the waters on the cold side of the front makes

ascribing the presence of these blooms to local (rather than coastal upwelling) dynamics tenuous. Still, both Dewey *et al.* (1991) and Strub *et al.* (1991) described local upwelling within the front that was apparently not due to the original coastal upwelling forcing. Rather, surface wind-driven mixing and local adjustments in relative vorticity led to cross-frontal isopycnal upwelling and downwelling in a sense similar to that of Figure 5. Both Hood *et al.* and Chavez *et al.* report subsurface patches of enhanced chlorophyll on the warm side of the fronts. Hood *et al.* find considerable support for the argument that their subsurface patch was subducted from a surface population on the cold side of the front. Such dynamics were not reproduced by this model.

While this comparison of model and data is evocative, it is not a strong test of the model. A more compelling test would be a comparison of the model with time series obtained at fronts, including physical and biological measurements. Appropriate physical measurements were made in the FASINEX program (Weller, 1991), however, to our knowledge no comparable biological measurements have been made. Thus a strong test of this model and its predictions will await an appropriate field program. The largest biological signal would be expected at fronts with large cross-frontal nutrient gradients. Good examples of such fronts are found in temperate waters such as the Skagerrak/Kattegat region (e.g., Heilmann *et al.,* 1994), and the Almeria-Oran front of the Mediterranean (e.g., Prieur and Sournia, 1994).

The first-order response of the phytoplankton to the wind events at the front was enhanced growth on the cold side fueled by the vertical mixing of nutrients. After this bloom decayed, however, the continuing production was centered at the front around the pycnocline. This production would be invisible to satellite remote sensing, since most of the signal received by a satellite color sensor originates in the upper optical depth of the ocean (Gordon and Clark, 1980). The subsurface blooms simulated in the present model occur deeper than one optical depth, and represent a significant spatial nonuniformity in the phytoplankton biomass. While there is often a good correlation of surface chlorophyll with integrated chlorophyll or primary production (e.g., Smith, 1981; Sathyendranath and Platt, 1989), this relationship is likely to break down in regions with strong cross-frontal nutrient gradients due to the subsurface patchiness of phytoplankton populations. Thus the satellite would accurately record the surface blooms of phytoplankton in the colder, nutrient-rich waters after a wind event, but would miss the more enduring subsurface phytoplankton patch, and therefore underestimate the fraction of production related to frontal dynamics.

Many of the conclusions obtained from this modeling study are general and should apply to many different types of front. The conclusion regarding the interaction of sinking and cross-frontal circulations in leading to accumulation of biomass, however, is specific to the particular initial conditions used in this study. The cross-frontal circulation pattern used to examine this issue was generated by the diffusion of the strong temperature gradients of the initial physical fields. The circulation was weak, and is probably not a good representation of the cross-frontal flow patterns developed by forced three-dimensional fronts. Cross-frontal flows generated in along-front meanders and instabilities can have significant

effects on the primary and secondary production (e.g., Flierl and Davis, 1993; Lohrenz *et al.,* 1993; Hitchcock *et al.,* 1993), but cannot be reproduced by the present two-dimensional model. The lack of a vertical dependence of sinking speed in the present model precluded accumulation *per se* (Franks, 1992b), and sinking did not contribute significantly to the formation of the subsurface phytoplankton patch. Less conservative sinking behaviors, such as a decreased sinking speed in nutrient-rich waters (Bienfang *et al.,* 1982), or a growth-rate-dependent sinking speed could lead to a more pronounced effect of cross-frontal flows on phytoplankton patchiness.

We did not include a surface buoyancy flux in the model, in the interest of keeping the model simple. In a modeling study of wind and buoyancy forcing of a similar front, Pereira and Mascarenhas (1994) found that leaving out buoyancy forcing did not significantly change the mixed-layer depths and velocities during the wind event, and the oscillations of the front were unchanged after the wind event. Dewey and Moum (1990) found that wind mixing was a predominant source of dissipation of turbulent kinetic energy in the surface waters of a front, with an extremely rapid (~1 hour) response of mixing-layer depth to changes in wind stress. Differences in the depth of the pycnocline across the front accounted for the observed differences in wind-driven buoyancy fluxes across the front. Thus we have probably included the most significant forcings of frontal mixed layers in our model.

The cross-frontal flows simulated in the present model are a result of strictly two-dimensional cross-frontal dynamics. In reality, fronts are not perfectly linear features, but have along-front waves and instabilities. These features arise through the three-dimensional dynamics, and can drive strong cross-frontal flows (e.g., Bower and Rossby, 1989) and fluxes (James, 1988). The vertical flows driven by frontal meanders can drive significant patchiness of biological fields (Flierl and Davis, 1993; Hitchcock *et al.,* 1993; Lohrenz *et al.,* 1993), however, the interaction of such flows with wind-forcing of the surface mixed layer has not been explored. The model presented here is an ideal vehicle for exploring such phenomena in future studies.

Acknowledgments. We thank David Adamec for making his code available to us for this study. This paper is funded in part by grant NA36GP0320 to PJSF from the National Oceanic and Atmospheric Administration, and a postdoctoral fellowship from the University Corporation for Atmospheric Research. LJW was funded through the Coastal Dynamics Program of ONR through grant N00014-92-J-1018 to Oregon State University. The views expressed herein are those of the authors and do not necessarily reflect the views of NOAA or any of its subagencies. This is contribution no. 73 of the U.S. GLOBEC program, funded jointly by NOAA and NSF.

REFERENCES

Adamec, D., R. L. Elsberry, R. W. Garwood, Jr. and R. L. Haney. 1981. An embedded mixed-layer-ocean circulation model. Dyn. Atm. Oceans, *6,* 69–96.

Bianchi, M., P. Morin and P. Le Corre. 1994. Nitrification rates, nitrite and nitrate distribution in the Almeria-Oran frontal systems (eastern Alboran Sea). J. Mar. Syst., *5,* 327–342.

Bienfang, P. K., P. J. Harrison and L. M. Quarmby. 1982. Sinking rate response to depletion of nitrate, phosphate and silicate in four marine diatoms. Mar. Biol., *647,* 295–302.

Boucher, J., F. Ibanez and L. Prieur. 1987. Daily and seasonal variations in the spatial distribution of zooplankton populations in relation to the physical structure in the Ligurian Sea front. J. Mar. Res., *45,* 133–173.

Bower, A. S. and T. Rossby. 1989. Evidence of cross-frontal exchange processes in the Gulf Stream based on isopycnal RAFOS float data. J. Phys. Oceanogr., *19,* 1177–1190.

Brink, K. H. and T. J. Cowles. 1991. The coastal transition zone program. J. Geophys. Res., *96,* 14,637–14,647.

Chavez, F. P., R. T. Barber, P. M. Kosro, A. Huyer, S. R. Ramp, T. P. Stanton and B. Rojas de Mendiola. 1991. Horizontal transport and the distribution of nutrients in the Coastal Transition Zone off Northern California: effects on primary production, phytoplankton biomass and species composition. J. Geophys. Res., *96,* 14,833–14,848.

Claustre, H., P. Kerhervé, J.-C. Marty and L. Prieur. 1994a. Phytoplankton photoadaptation related to some frontal physical processes. J. Mar. Syst., *5,* 251–265.

Claustre, H., P. Kerhervé, J.-C. Marty, L. Prier, C. Videau and J.-H. Hecq. 1994b. Phytoplankton dynamics associated with a geostrophic front: Ecological and biogeochemical implications. J. Mar. Res., *52,* 711–742.

Dewey, R. K. and J. N. Moum. 1990. Enhancement of fronts by vertical mixing. J. Geophys. Res., *95,* 9433–9445.

Dewey, R. K., J. N. Moum, C. A. Paulson, D. R. Caldwell and S. D. Pierce. 1991. Structure and dynamics of a coastal filament. J. Geophys. Res., *96,* 14,885–14,907.

Dippner, J. W. 1993. A Lagrangian model of phytoplankton growth dynamics for the Northern Adriatic Sea. Cont. Shelf Res., *13,* 331–355.

Dugdale, R. C. and J. J. Goering. 1967. Uptake of new and regenerated forms of nitrogen in primary productivity. Limnol. Oceanogr., *12,* 196–206.

Eppley, R. W. 1992. Chlorophyll, photosynthesis and new production in the Southern California Bight. Prog. Oceanogr., *30,* 117–150.

Eppley, R. W. and B. J. Peterson. 1979. Particulate organic matter flux and planktonic new production in the deep ocean. Nature, *282,* 677–680.

Eppley, R. W. and E. H. Renger. 1988. Nanomolar increase in surface layer nitrate concentration following a small wind event. Deep-Sea Res., *35,* 1119–1125.

Eppley, R. W., E. H. Renger and W. G. Harrison. 1979. Nitrate and phytoplankton production in Southern California Coastal waters. Limnol. Oceanogr., *24,* 483–494.

Eriksen, C. C., R. A. Weller, D. L. Rudnick, R. T. Pollard and L. A. Regier. 1991. Ocean frontal variability in the Frontal Air-Sea Interaction Experiment. J. Geophys. Res., *96,* 8,569–8,591.

Fasham, M. J. R., H. W. Ducklow and S. M. McKelvie. 1990. A nitrogen-based model of plankton dynamics in the oceanic mixed layer. J. Mar. Res., *48,* 591–639.

Fasham, M. J. R., T. Platt, B. Irwin and K. Jones. 1985. Factors affecting the spatial pattern of the deep chlorophyll maximum in the region of the Azores Front. Prog. Oceanogr., *14,* 129–165.

Flierl, G. R. and C. S. Davis. 1993. Biological effects of Gulf Stream meandering. J. Mar. Res., *51,* 529–560.

Franks, P. J. S. 1992a. Phytoplankton blooms at fronts: patterns, scales, and physical forcing mechanisms. Rev. Aquat. Sci., *6,* 121–137.

—— 1992b. Sink or swim: accumulation of biomass at fronts. Mar. Ecol. Prog. Ser., *82,* 1–12.

Franks, P. J. S., J. S. Wroblewski and G. R. Flierl. 1986. Behavior of a simple plankton model with food-level accumulation by herbivores. Mar. Biol., *91,* 121–129.

Garwood, R. W., Jr. 1977. An oceanic mixed layer model capable of simulating cyclic states. J. Phys. Oceanogr., *7,* 455–468.

Gill, A. E. 1982. Atmosphere-Ocean Dynamics, Academic Press, New York, NY, 662 pp.

Gordon, H. R. and D. K. Clark. 1980. Remote sensing optical properties of a stratified ocean: an improved interpretation. Appl. Optics, *19,* 3428–3430.

Heilmann, J. P., K. Richardson and G. Ærtbjerg. 1994. Annual distribution and activity of phytoplankton in the Skagerrak/Kattegat frontal regions. Mar. Ecol. Prog. Ser., *112,* 213–223.

Hitchcock, G. L., A. J. Mariano and T. Rossby. 1993. Mesoscale pigment fields in the Gulf Stream: observations in a meander crest and trough. J. Geophys. Res., *948,* 8425–8445.

Holligan, P. M. 1981. Biological implications of fronts on the northwest European continental shelf. Phil. Trans. R. Soc. Lond., *A302,* 547–562.

Holligan, P. M., P. J. leB. Williams, D. Purdie and R. P. Harris. 1984. Photosynthesis, respiration and nitrogen supply of plankton populations in stratified, frontal and tidally mixed shelf waters. Mar. Ecol. Prog. Ser., *17,* 201–213.

Holloway, G. and K. Denman. 1989. Influence of internal waves on primary production. J. Plankton Res., *11,* 409–413.

Hood, R. R., M. R. Abbott and A. Huyer. 1991. Phytoplankton and photosynthetic light response in the coastal transition zone off northern California in June 1987. J. Geophys. Res., *96,* 14,769–14,780.

Houghton, R. W. and J. Marra. 1983. Physical/biological structure and exchange across the thermohaline shelf/slope front in the New York Bight. J. Geophys. Res., *88,* 4467–4481.

Huyer, A., P. M. Kosro, J. Fleischbein, S. R. Ramp, T. Stanton, L. Washburn, F. P. Chavez, T. J. Cowles, S. D. Pierce and R. L. Smith. 1991. Currents and water masses of the Coastal Transition Zone off northern California in June 1987. J. Geophys. Res., *96,* 14,809–14,831.

James, I. D. 1988. Experiments with a numerical model of coastal currents and tidal mixing fronts. Cont. Shelf Res., *8,* 1275–1297.

Karhu, M., S. Nômmann and B. Zeitzschel. 1991. Particle (plankton) size structure across the Azores Front (Joint Global Ocean Flux Study North Atlantic Bloom Experiment). J. Geophys. Res., *96,* 7,083–7,088.

Klein, P. and B. Coste. 1984. Effects of wind-stress variability on nutrient transport into the mixed layer. Deep-Sea Res., *31,* 21–37.

Kokkinakis, S. A. and P. A. Wheeler. 1987. Nitrogen uptake and phytoplankton growth in coastal upwelling regions. Limnol. Oceanogr., *32,* 1,112–1,123.

Kosro, P. M., A. Huyer, S. R. Ramp, R. L. Smith, F. P. Chavez, T. J. Cowles, M. R. Abbott, P. T. Strub, R. T. Barber, P. Jessen and L. F. Small. 1991. The structure of the transition zone between coastal waters and the open ocean off northern California, winter and spring. 1987. J. Geophys. Res., *96,* 14,707–14,730.

Lohrenz, S. E., J. J. Cullen, D. A. Phinney, D. B. Olson and C. S. Yentsch. 1993. Distributions of pigments and primary production in a Gulf Stream meander. J. Geophys. Res., *948,* 14,545–14,560.

Marra, J., R. W. Houghton and C. Garside. 1990. Phytoplankton growth at the shelf-break front in the Middle Atlantic Bight. J. Mar. Res., *48,* 851–868.

Mitchell-Innes, B. A. and D. R. Walker. 1991. Short-term variability during an anchor station study in the southern Benguela upwelling system: phytoplankton production and biomass in relation to species changes. Prog. Oceanogr., *28,* 65–89.

Niiler, P. P. 1969. On the Ekman divergence in an oceanic jet. J. Geophys. Res., *74,* 7048–7052.

Orlanski, I. 1976. A simple boundary condition for unbounded hyperbolic flows. J. Comp. Phys., *21,* 251–269.

Pereira, C. S. and A. da S. Mascarenhas Jr. 1994. Numerical simulation of a response of an oceanic front to an atmospheric frontal passage. J. Geophys. Res., *99,* 16081–16094.

Pingree, R. D., P. M. Holligan and G. T. Mardell. 1978. The effects of vertical stability on phytoplankton distributions in the summer on the northeast European shelf. Deep-Sea Res., *25,* 1011–1028.

Price, J. F. 1983. Internal wave wake of a moving storm. Part 1: Scales, energy budget and observations. J. Phys. Oceanogr., *13,* 949–965.

Prieur, L. and A. Sournia. 1994. Almofront-1 (April-May 1991): an interdisciplinary study of the Almeria-Oran geostrophic front, SW Mediterranean Sea. J. Mar. Syst., *5,* 187–203.

Ruan, S. 1993. Persistence and coexistence in zooplankton-phytoplankton-nutrient models with instantaneous nutrient cycling. J. Math. Biol., *31,* 633–654.

Sathyendranath, S. and T. Platt. 1989. Remote sensing of ocean chlorophyll: consequence of nonuniform pigment profile. Appl. Optics, *28,* 490–495.

Small, L. F. and D. W. Menzies. 1981. Patterns of primary productivity and biomass in a coastal upwelling zone. Deep-Sea Res., *28A,* 123–149.

Smith, R. C. 1981. Remote sensing and depth distribution of ocean chlorophyll. Mar. Ecol. Prog. Ser., *5,* 359–361.

Steele, J. H. and E. W. Henderson. 1992. The role of predation in plankton models. J. Plankton Res., *14,* 157–172.

Strub, P. T., P. M. Kosro and A. Huyer. 1991. The nature of the cold filaments in the California Current System. J. Geophys. Res., *96,* 14,743–14,768.

Traganza, E. D., D. G. Redalje and R. W. Garwood. 1987. Chemical flux, mixed layer entrainment and phytoplankton blooms at upwelling fronts in the California coastal zone. Cont. Shelf Res., *7,* 89–105.

Videau, C., A. Sournia, L. Prieur and M. Fiala. 1994. Phytoplankton and primary production characteristics at selected sites in the geostrophic Almeria-Oran front system (SW Mediterranean Sea). J. Mar. Syst., *5,* 235–250.

Waldron, H. N. and T. A. Probyn. 1991. Short-term variability during an anchor station study in the southern Benguela upwelling system: nitrogen supply to the euphotic zone during a quiescent phase in the upwelling cycle. Prog. Oceanogr., *28,* 153–166.

Walstad, L. J. and A. R. Robinson. 1993. A coupled surface boundary-layer quasigeostrophic model. Dyn. Atm. Oceans, *18,* 151–207.

Washburn, L., D. C. Kadko, B. H. Jones, T. Hayward, P. M. Kosro, T. P. Stanton, S. Ramp and T. Cowles. 1991. Water mass subduction and the transport of phytoplankton in a coastal upwelling system. J. Geophys. Res., *96,* 14,927–14,945.

Weller, R. A. 1991. Overview of the Frontal Air-Sea Interaction Experiment (FASINEX): a study of air-sea interaction in a region of strong oceanic gradients. J. Geophys. Res., *96,* 8,501–8,516.

Wroblewski, J. S., J. L. Sarmiento and G. R. Flierl. 1988. An ocean basin scale model of plankton dynamics in the North Atlantic 1. Solutions for the climatological oceanographic conditions in May. Global Biogeochem. Cycles, *2,* 199–218.

Yentsch, C. S. 1974. The influence of geostrophy on primary production. Tethys, *6,* 111–118.

Received: *24 April, 1996;* revised: *4 September, 1996.*